Mechanical Activation of α-AlF_3: Changes in Structure and Reactivity

G. Scholz,*,† R. König,† J. Petersen,† B. Angelow,† I. Dörfel,‡ and E. Kemnitz†

Institut für Chemie, Humboldt-Universität zu Berlin, D-12489 Berlin, Germany, and Bundesanstalt für Materialforschung und – prüfung, D-12205 Berlin, Germany

Received March 6, 2008. Revised Manuscript Received June 17, 2008

α-AlF_3, the thermodynamically stable rhombohedral phase of aluminum fluoride, was used as starting material to produce nanostructured powders by high-energy ball milling. Both the polycrystalline and the nanostructured powders were studied by XRD, TEM, and ^{27}Al and ^{19}F MAS NMR. Thermally programmed desorption of NH_3 and IR spectroscopy of adsorbed CO probe molecules unambiguously demonstrate the formation of Lewis acid and Brønsted acid sites as a consequence of the mechanical impact. Catalytic test reactions using milled α-AlF_3 as solid catalyst proved experimentally the theoretically suggested catalytic activity of nanosized AlF_3 particles as a result of high structural distortion brought into the solid by milling.

1. Introduction

In the field of heterogeneous catalysis it is of tremendous importance to use high-surface inorganic materials as catalysts, since the activity of catalysts essentially depends on their large surface accompanied by a high degree of distortion. Solid metal fluorides like, for example, β-MF_3 (M: Al, Cr, Fe, V), are well known Lewis acid catalysts for halogen exchange reactions.[1–4] Different attempts were undertaken to obtain seriously distorted or amorphous AlF_3 with high surface as well as other binary metal fluorides following aqueous[2] and non-aqueous synthesis strategies.[5,6] Meanwhile, amorphous high-surface area aluminum fluoride can be prepared with a Lewis acidity comparable to antimony pentafluoride via a sol−gel synthesis route.[6,7] Besides the sol−gel route, a further way of synthesis of high-surface AlF_3 is the plasma-assisted fluorination reaction of zeolites as published in ref 8.

A possible alternative route for the preparation of reactive surfaces and nano-sized particles is high-energy ball milling.

In contrast to oxide compounds (e.g., refs 9–13) the mechano-chemical approach of a distortion of the original polycrystalline sample by high-energy ball-milling has been less regarded so far for solid fluorides (see, e.g., refs 14–17). Our own milling experiments with solid fluorides (crystalline CaF_2[18] and milling of NaF with AlF_3 [19,20] demonstrated the potential of mechanical milling regarding structural and reactivity changes also for this class of compounds.

In the present contribution, the well-known thermodynamically stable rhombohedral phase of aluminum fluoride, α-AlF_3,[21,22] was chosen as a reference system to study the effect of a mechanical impact on solid fluorides. Its crystal structure (α-AlF_3, space group $R\bar{3}c$) consists of corner-shared $\{AlF_6\}$ octahedra forming a three-dimensional network as illustrated in Figure 1a. As shown by X-ray, differential scanning calorimetry (DSC), Raman, and electron paramagnetic resonance (EPR) measurements, the matrix undergoes a phase transition of first order at $T_c = 729$ K.[22–25]

* Corresponding author. E-mail: Gudrun.Scholz@rz.hu-berlin.de.
† Humboldt-Universität zu Berlin.
‡ Bundesanstalt für Materialforschung und prüfung.

(1) Kemnitz, E.; Menz, D.-H. *Progr. Solid State Chem.* **1998**, *26*, 97.
(2) Kemnitz, E.; Zhu, Y.; Adamczyk, B. *J. Fluorine Chem.* **2002**, *114*, 163.
(3) Kemnitz, E.; Winfield, J. M. In *Advanced Inorganic Fluorides: Synthesis, Characterization and Applications*; Nakajima, T., Tressaud, A., Zemva, B., Eds.; Elsevier Science S.A.: Amsterdam, 2000; p 367.
(4) Böse, O.; Adamczyk, B.; Fiedler, K.; Kemnitz, E. *Catal. Lett.* **1998**, *54*, 211.
(5) Kemnitz, E.; Gross, U.; Rüdiger, S.; Shekar, C. S. *Angew. Chem.* **2003**, *115*, 4383.
(6) Rüdiger, S.; Eltanany, G.; Gross, U.; Kemnitz, E. *J. Sol-Gel Sci. Technol.* **2007**, *41*, 299.
(7) Christe, K. O.; Dixon, D. A.; McLemore, D.; Wilson, W. W.; Sheehy, J. A.; Boatz, J. A. *J. Fluorine Chem.* **2000**, *101*, 151.
(8) Delattre, J. L.; Chupas, P. J.; Grey, C. P.; Stacy, A. M. *J. Am. Chem. Soc.* **2001**, *123*, 5364.
(9) Scholz, G.; Stösser, R.; Klein, J.; Silly, G.; Buzaré, J. Y.; Laligant, Y.; Ziemer, B. *J. Phys.: Condens. Matter* **2002**, *14*, 2101.
(10) Buzaré, J.Y.; Silly, G.; Klein, J.; Scholz, G.; Stösser, R.; Nofz, M. *J. Phys.: Condens. Matter* **2002**, *14*, 10331.
(11) Gaffet, E.; Michel, D.; Mazerolles, L.; Berthet, P. *Mater. Sci. Forum* **1997**, *235−238*, 103.
(12) Mackenzie, K. J. D.; Temuujin, J.; Jadambaa, T.; Smith, M. E.; Angerer, P. *J. Mater. Sci.* **2000**, *35*, 5529.
(13) Nakano, T.; Kamitani, M.; Senna, M. *Mater. Sci. Forum* **1996**, *225−227*, 587.
(14) Uno, M.; Onitsuka, M.; Ito, Y.; Yoshikado, S. *Solid State Ionics* **2005**, *176*, 2493.
(15) Guérault, H.; Tamine, M.; Greneche, J. M. *J. Phys.: Condens. Matter* **2000**, *12*, 9497.
(16) Guérault, H.; Greneche, J. M. *J. Phys.: Condens. Matter* **2000**, *12*, 4791.
(17) Bureau, B.; Guérault, H.; Silly, G.; Buzaré, J. Y.; Greneche, J. M. *J. Phys.: Condens. Matter* **1999**, *11*, L423.
(18) Scholz, G.; Dörfel, I.; Heidemann, D.; Feist, M.; Stösser, R. *J. Solid State Chem.* **2006**, *179*, 1119.
(19) Scholz, G.; Korup, O. *Solid State Sci.* **2006**, *8*, 678.
(20) Scholz, G.; Feist, M.; Kemnitz, E. *J. Solid State Sci.* **2008**, DOI: 10.1016/j. solidstatesciences.2008.03.008.
(21) Ravez, J.; Mogus-Milankovic, A.; Chaminade, J. P.; Hagenmuller, P. *Mater. Res. Bull.* **1984**, *19*, 1311.
(22) Daniel, P.; Bulou, A.; Rousseau, M.; Nouet, J.; Fourquet, J. L.; Leblanc, M.; Burriel, R. *J. Phys.: Condens. Matter* **1990**, *2*, 5663.
(23) Daniel, P.; Bulou, A.; Rousseau, M.; Nouet, J. *Phys. Rev.* **1990**, *B42*, 10545.
(24) Daniel, P. Thesis, Université du Maine, Le Mans, France, 1990.

10.1021/cm801135h CCC: $40.75
Published on Web 07/29/2008

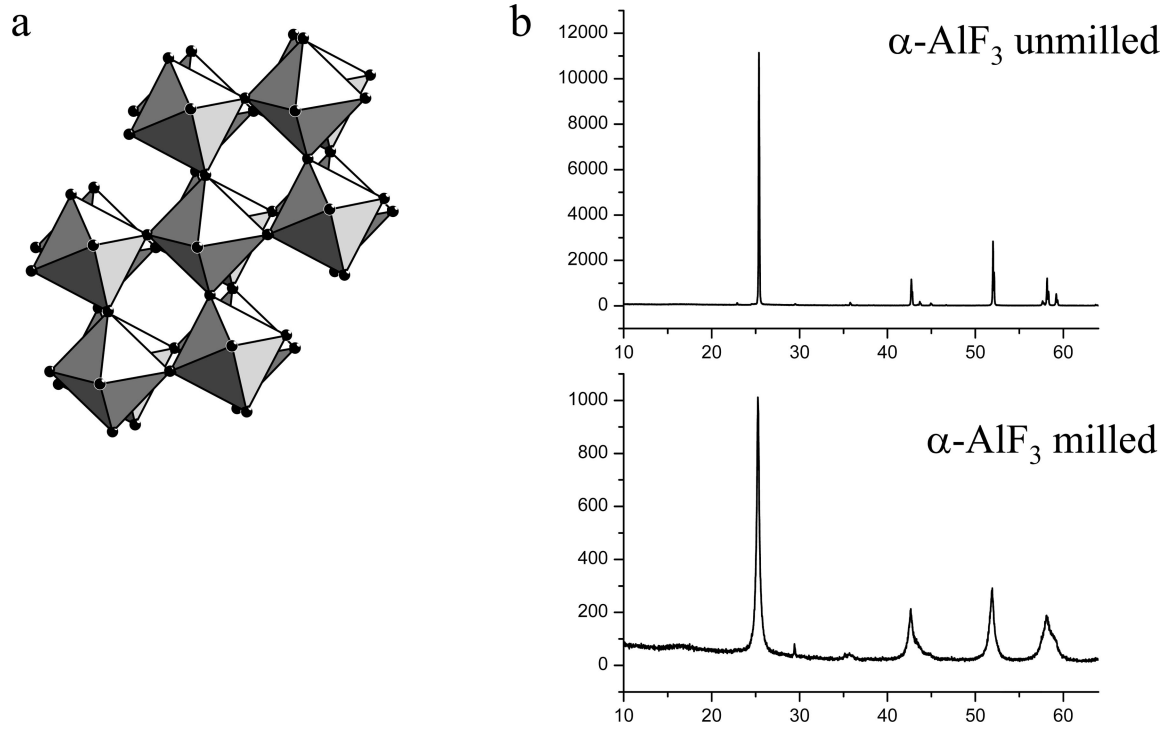

Figure 1. Structure model of crystalline α-AlF_3 (a) and X-ray powder patterns of unmilled and air-milled α-AlF_3 samples (b). (Milling under dry and air conditions leads to almost identical powder diffractograms as given in (b); the sharp peak at $2\theta \sim 29°$ is caused by the sample holder.)

On the basis of surface thermodynamics calculations using hybrid-exchange density functional theory it was shown that the surface of α-AlF_3 is terminated by a layer containing two F^- ions forming a zigzag chain across the surface.[26] As a consequence the Al^{3+} ions, which might in general act as Lewis acid sites, are masked by the surrounding environment. Therefore, and in accordance with former experimental observations,[2,3] α-AlF_3 is not able to act as a Lewis acid catalyst.

On the other hand, atomistic molecular dynamics simulations of *cubic nanoparticles* of α-AlF_3 revealed the formation of Lewis acid sites present at corners and edges of the nanoparticles.[27] The postulated Lewis acidity is assumed to be due to high numbers of 5- and 4-fold coordinated sites on the surface of the nanoparticles. These calculations [26,27] illustrate how structures and properties of surface sites of *nanoparticles* can be quite different from those predicted from models derived from the *crystalline* bulk stucture considering infinite periodic surfaces.

Mechanical milling with the known effect of decreasing the particle size may bridge the gap between different theoretical approaches describing the surface structure of crystalline and nanosized α-AlF_3 particles.

Therefore, starting with the crystalline powder α-AlF_3, it is the intention of the present work (i) to follow structural changes at mechanical activation of α-AlF_3, (ii) to study a possible formation of surface acid sites at milling, and (iii) to test the catalytic activity of as-prepared nanosized samples.

X-ray diffraction (XRD), transmission electron microscopy (TEM), and magic angle spinning (MAS) NMR methods were applied for structure characterization, whereas adsorption/desorption techniques as well as a catalytic test reaction were applied to study the formation, the kind, and strength of surface acid sites.

2. Experimental Details

Milling. Powder samples of α-AlF_3 were prepared from α-$AlF_3 \cdot 3H_2O$ in special Q-crucibles at 1000 °C for 1 h in a furnace (Thermolyne). In addition, a commercial powder sample of α-AlF_3 (Aldrich) was used for comparison. Aluminum fluoride trihydrate was prepared according to ref 28 by precipitation. The aluminum fluoride powder was milled in a commercial planetary mill "Pulverisette 7" (Fritsch, Germany) applying both normal (air) and inert conditions (Ar atmosphere). Five syalon balls were used in each syalon vial ($m_{balls} = 14.8$g; $m_{sample} = 1$ g). The rotational speed of 600 rpm was chosen together with a milling time of 4 h as standard procedure.

XRD. XRD measurements were performed using the FPM 7 equipment (Rich. Seiffert & Co., Freiberg) with Cu Kα (Cu $K\alpha_{1,2}$, $\lambda = 1.5418$ Å) radiation (2Θ range, $5° \leq 2\Theta \leq 64°$; step scan, 0.05°; step time, 5 s). Phases were identified by comparison with the ICSD powder diffraction file.[29]

TEM. The TEM study was performed with a 200 kV CM20 microscope and a 400 kV JEOL 4000FX microscope. Electron diffraction investigations were combined with EDX examinations for the characterization of the samples. The samples were prepared by depositing a few droplets of a suspension of the powders in alcohol on a carbon coated copper grid.

MAS NMR. ^{27}Al and ^{19}F MAS NMR spectra were recorded on a Bruker Avance 400 spectrometer with 2.5 mm and 4 mm probes and the respective zirconia rotors.

(25) Scholz, G.; Stösser, R.; Buzaré, J. Y.; Legein, Ch.; Silly, G. *Appl. Magn. Res.* **2000**, *18*, 199.
(26) Wander, A.; Searle, B. G.; Bailey, C. L.; Harrison, N. M. *J. Phys. Chem. B* **2005**, *109*, 22935.
(27) Chaudhuri, S.; Chupas, P.; Morgan, B. J.; Madden, P. A.; Grey, C. P. *Phys. Chem. Chem. Phys.* **2006**, *8*, 5045.
(28) Schmidt, A. *Monatsh. Chem.* **1967**, *98*, 482.
(29) Powder Diffraction File, ICPDS-ICDD2001.

^{19}F MAS NMR ($I = 1/2$) spectra were recorded with a $\pi/2$ pulse duration of p1 = 2 μs, a spectrum width of 400 kHz, a recycle delay of 10 s, and an accumulation number of 64 and applying a spinning speed of 30 kHz. The ^{19}F spin lattice relaxation time of unmilled and milled samples was determined with the inversion recovery technique.[30] The isotropic chemical shifts δ_{iso} of ^{19}F resonances are given below with respect to the $CFCl_3$ standard. Existent background signals of ^{19}F could be completely suppressed with the application of a phase-cycled depth pulse sequence according to Cory and Ritchey.[31]

^{27}Al MAS NMR spectra taken with the 2.5 mm probe were recorded with a MAS frequency of 25 kHz, an excitation pulse duration of 1 μs, a recycle delay of 1 s, and an accumulation number of 7200. ^{27}A1-{^{19}F}-cw-decoupling experiments for crystalline and nanosized samples were performed at a MAS frequency of 3 kHz.

A 1 M aqueous solution of $AlCl_3$ was used as reference for the chemical shift of ^{27}A1. The ^{19}F and ^{27}Al MAS NMR spectra were calculated with the program DMFIT.[32]

Differential Thermal Analysis/Thermogravimetry (DTA-TG). Both the unmilled and air-milled AlF_3 samples were studied using DTA-TG measurements in a Netzsch STA 409C/CD thermobalance (heating rate, 10 K/min under N_2 up to 800 °C).

NH_3-TPD. Temperature-programmed desorption (TPD) of ammonia (NH_3-TPD) was employed to determine the presence and strength of acid sites of both milled and unmilled samples. The samples (about 0.2 g) were first heated under Ar up to 400 °C (10 K/min) and kept at 400 °C for 1 h, cooling down to 120 °C and exposing to NH_3. After cooling down to 80 °C and flushing physisorbed ammonia with Ar for about 30 min, the TPD program was started (7.5 K/min up to 475 °C, keeping the temperature at 475 °C for 30 min). Desorbed ammonia was continuously monitored using IR spectroscopy (FT-IR system 2000, Perkin-Elmer).

CO Adsorption. IR spectroscopy of CO adsorbed on surfaces of milled α-AlF_3 samples was performed using the cell and spectrometer as described in ref 33. The degassing of the samples was performed using (i) the standard degassing procedure as given in ref 33 and (ii) evacuating the milled samples at 90 °C for 12 h to avoid reorganization and grain growth in the matrix.

Catalytic Test Reaction. To test the Lewis acidity of milled α-AlF_3 samples the dismutation reaction of $CHClF_2$ was used as the probe reaction. The reaction according to the general eq 1

$$5CHClF_2(g) \rightarrow CHCl_2F(g) + 3CHF_3(g) + CHCl_3(g) \quad (1)$$

proceeds only in the presence of Lewis acidic catalysts.[1] The reaction was performed in a flow reactor (Ni tube) located vertically in an electrical furnace (see also ref 6). About 0.3 g of the sample was positioned on a silver wool plug. A constant gas flow of $CHClF_2$ (5 mL/min) and diluting N_2 (20 mL/min) was adjusted. The reaction was followed at four temperatures (150 °C, 200 °C, 250 °C, 300 °C) waiting for 2 h at every temperature to ensure the thermal equilibrium. The product composition was analyzed online by gas chromatography.

3. Results

Together with a structure model (Figure 1a) the X-ray powder diffractograms of unmilled α-AlF_3 and of the samples milled for 4 h are depicted in Figure 1b. After milling for 4 h a distinct decrease of the amplitudes and a broadening of all reflections can be observed. No additional reflections appear. The powder patterns of the samples milled under dry conditions and in air are almost identical and therefore not separately shown. The observed effects are mainly due to the decrease of the grain sizes by milling. From high-resolution XRD powder patterns the mean grain size was determined to be 400 nm for the unmilled sample and 45 nm for the milled sample,[34] which is a reduction to about 1/10 of the original value.

The TEM micrographs of unmilled α-AlF_3 and dry-milled AlF_3 are given in Figure 2. Both the unmilled (Figure 2a) and the milled sample (Figure 2b) consist of the stable rhombohedral phase of α-AlF_3. Differences between the two samples can be found only in the particle size and particle shape. The starting material contains irregularly formed particles up to needles ranging from 100 nm to 10 μm in size (Figure 2a).

The milled sample consists of particles with a distinctly diminished size beginning with 10 nm, and only a few number in the range of 200−400 nm (Figure 2). The smaller particles are spherically shaped. Even the very small particles consist of nanocrystalline α-AlF_3, and an amorphization could not be established applying the present milling conditions.

The ^{27}A1 NMR parameters of crystalline α-AlF_3 (s.ee also Figure 3a) were accurately determined previously by simulation of the spectra taken at a spinning speed of 3 kHz.[19] The best simulation was achieved with the values $\delta_i = -15.5$ ppm (isotropic chemical shift value), $\nu_Q = 31.8$ kHz (ν_Q: quadrupolar frequency), and $\eta_Q = 0$[19] (η_Q: asymmetry parameter) which are close to values obtained by Silly et al.[35] and Chupas et al.[36]

Figure 4 shows changes in the ^{27}A1 and ^{19}F MAS NMR spectra as a result of milling and applying spinning speeds of 25 kHz and 30 kHz, respectively.

It is obvious that in the bulk no alteration of the six-fold coordination of the Al^{3+} ions is observable at milling applying the higher spinning speed. No extra lines appear, which would be characteristic for a four - or five-fold coordination of aluminum. This holds for samples milled both under dry conditions and in air, even performing ^{27}A1 high-field NMR measurements at 17.6 T. However, as shown with the 3 kHz and 25 kHz MAS measurements, milling has a remarkable effect on the spread and the shape of the envelope of the spinning side bands (cf. Figures 3 and 4) which is due to an increase of the quadrupolar frequency larger than 32 kHz as given for bulk α-AlF_3 above. A correct simulation of such a spectrum should imply statistical distributions of at least the quadrupolar frequency. A maximum value of the

(30) Mehring, M.; Weberruss, V. A. *Object-oriented Magnetic Resonance*; Academic Press: New York, 2001.
(31) Cory, D. G.; Ritchey, W. M. *J. Magn. Res.* **1988**, *80*, 128.
(32) Massiot, D.; Fayon, F.; Capron, M.; King, I.; Le Calvé, S.; Alonso, B.; Durand, J. O.; Bujoli, B.; Gan, Z.; Hoatson, G. *Magn. Reson. Chem.* **2002**, *40*, 70.
(33) Krahl, T.; Vimont, A.; Eltanany, G.; Daturi, M.; Kemnitz, E. *J. Phys. Chem. C* **2007**, *111*, 18317.
(34) Body, M. Université du Maine, Le Mans, personal communication.
(35) Silly, G.; Legein, Ch.; Buzaré, J. Y.; Calvayrac, F. *Solid State Nucl. Res.* **2004**, *25*, 241.
(36) Chupas, P. J.; Ciraolo, M. F.; Hanson, J. C.; Grey, C. P. *J. Am. Chem. Soc.* **2001**, *123*, 1694.

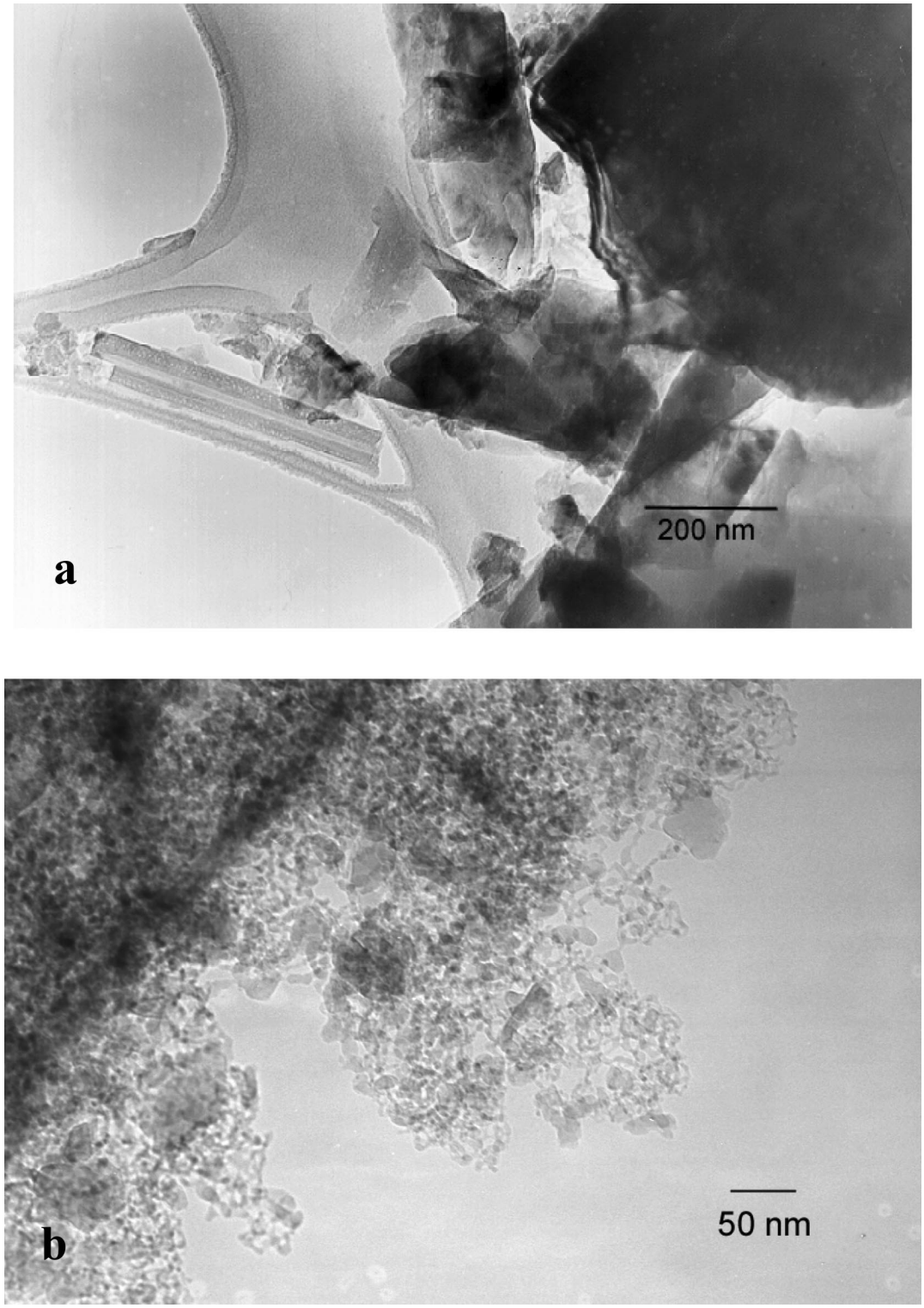

Figure 2. TEM micrographs of (a) unmilled crystalline α-AlF_3, showing needles and particles of different size and shape, and (b) α-AlF_3 milled for 16 h in a planetary mill with particles of a diameter of 50 nm and smaller.

quadrupolar frequency, determined by simulation from the spread of the spinning side bands, was determined as about 90 kHz.

The ^{19}F MAS NMR spectra show only marginal changes with milling. The isotropic chemical shift of ^{19}F in α-AlF_3 was determined to be $\delta_{iso} = -172.5$ ppm both for the milled and unmilled samples. The only change with milling is a low asymmetry in the low-field part of the spectrum. When a higher impact at milling in air is applied (not shown here), a shoulder at about −150 ppm appears which maybe assignable to μ-F in $AlF_{4/3}(OH/OH_2)_{2/3}$ on the surface.[37,38]

^{19}F MAS NMR spectra of air-milled and dry-milled samples are almost identical. Signals of very low intensity in the high-field part of the central line of the dry-milled

(37) Chupas, P. J.; Corbin, D. R.; Rao, V. N. M.; Hanson, J. C.; Grey, C. P. *J. Phys. Chem. B* **2003**, *107*, 8327.

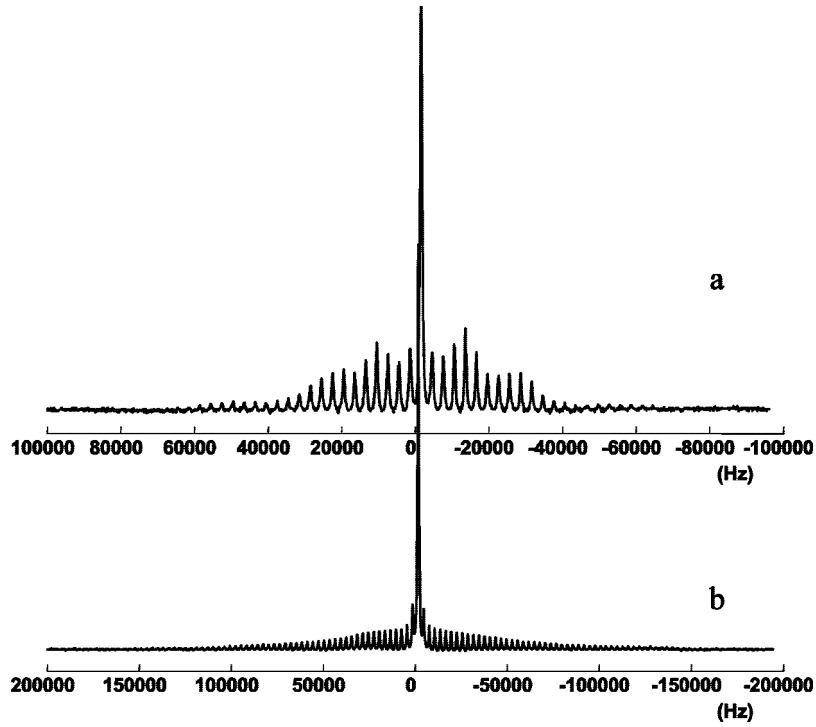

Figure 3. ^{27}Al-{^{19}F}-cw-decoupled MAS NMR spectra of unmilled (a) and 4 h milled α-AlF_3 (b), taken at 3 kHz spinning speed. (Note the doubled sweep width for spectrum b.)

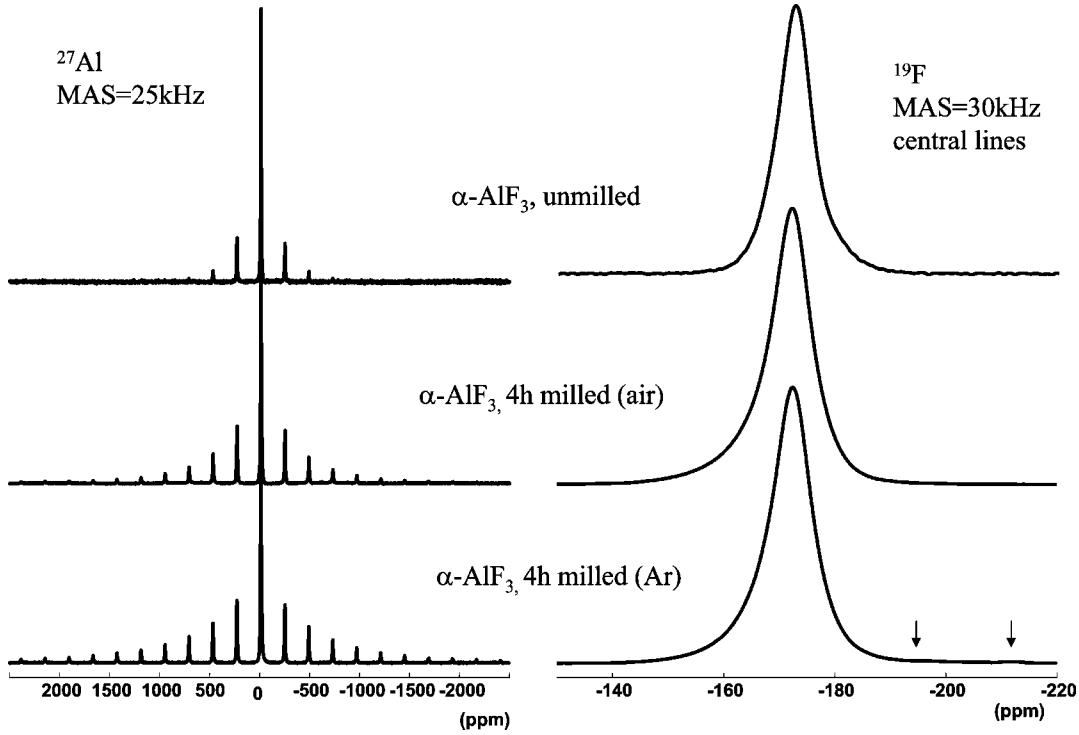

Figure 4. ^{27}Al and ^{19}F MAS NMR spectra of milled and unmilled α-AlF_3 samples recorded at high spinning speeds. (Arrows indicate signals of very low intensity.)

sample, however, might be correlated to terminal fluorine sites in the surface of nanoparticles.[39,42]

As already described for milled, nanocrystalline CaF_2 samples,[18] the ^{19}F spin lattice relaxation time T_1 allows a sensitive indication regarding the state of crystallinity and surface to bulk ratio. A T_1 value of 175.8 s was determined for crystalline α-AlF_3. This value diminishes to 5.4 s (3% of the original one) for a 16 h milled, nanocrystalline sample.

(38) Kemnitz, E.; Troyanov, S. I.; Morosov, I. V.; Gross, U.; Rüdiger, S.; Scholz, G.; Heidemann, D.; Lemée-Cailleau, M.-H. *Solid State Sci.* **2006**, *8*, 1443.

(39) Body, M.; Silly, G.; Legein, C.; Buzaré, J. Y. *Inorg. Chem.* **2004**, *43*, 2474.

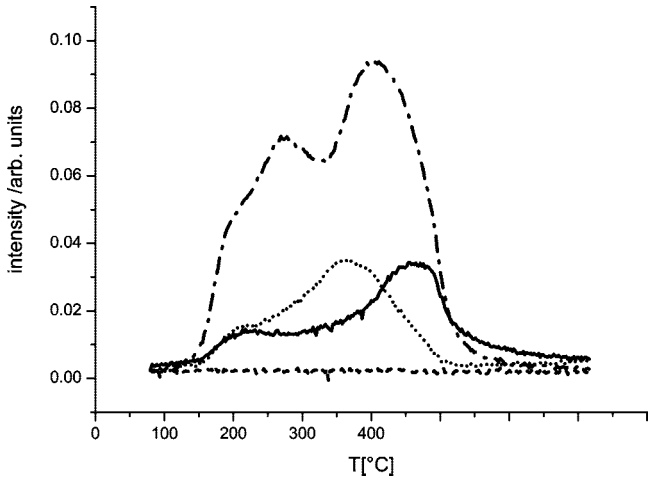

Figure 5. NH_3-TPD desorption profiles of milled and unmilled α-AlF_3 samples: (dashed line) unmilled; (solid line) air milled, preheated at 400 °C; (dotted line) dry milled, preheated at 400 °C; (dashed-dotted line) air milled, evacuated (18 h at 90 °C, no additional preheating). (The temperature was increased up to 475 °C and then kept for 30 min.)

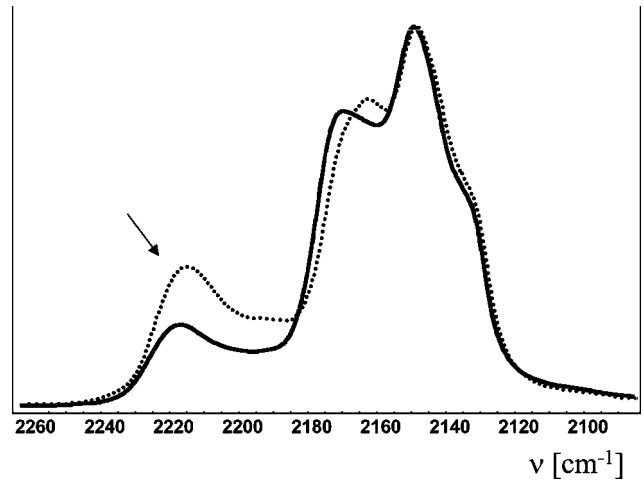

Figure 6. CO stretching region of absorption IR spectra of CO adsorbed on the surface of milled α-AlF_3 samples recorded after pre-treatment of the samples for 4 h at 300°C: (dotted line) dry milling; (solid line) air milling. (The difference between the pure sample and the sample with adsorbed CO is shown here. The arrow indicates the range of Lewis acid sites.)

Figure 5 (dashed line) gives clear evidence that the unmilled crystalline sample has no acid sites on its surface at all. The NH_3-TPD experiment clearly indicates that no ammonia has been adsorbed. On the other hand, for the milled samples there is no doubt concerning the existence of Brønsted and Lewis acid sites. Here, the desorption profiles differ depending on the kind and temperature of the thermal pre-treatment as well as on the milling procedure. A pre-treatment at 90 °C for 18 h in vacuum (0.002 μm Hg) results in a TPD area (Figure 5) which is 3.3 times larger than the areas obtained after a pre-treatment at 400 °C. In addition, the latter profiles show basically two main peaks in comparison to the three peaks recorded after treatment at 90 °C. Milling under dry conditions and preheating at 400 °C results in a comparable TPD area as obtained for the air milled product (see Figure 5). However, the strength of the acid sites is slightly decreased which is indicated by an almost finished desorption at 475 °C. It is interesting to note that the normalized TPD area calculated for the air- and dry-milled α-AlF_3 samples is comparable to that of β-AlF_3.[40]

For a discrimination between Lewis and Brønsted acid surface sites FT-IR spectroscopy after CO adsorption on the surfaces is a well established method.[33,41] In the present study, clear differences appear between samples milled under normal conditions (air) and under inert conditions (Figure 6). For the dry-milled sample the area calculated for the Lewis acid sites is doubled (see Figure 6).

The dismutation reactions of $CHClF_2$ using unmilled and milled α-AlF_3 samples as catalysts give clear evidence that crystalline α-AlF_3 is not at all active (Figure 7a). Although the BET areas of the milled samples are small (~16 m^2/g), they act as catalysts for reaction 1. At a temperature of 300 °C, the product gas phase consists of a mixture of mainly $CHCl_3$ and CHF_3. Even after cooling down to 40 °C the milled sample is still catalytically active (Figure 7b). Milling under dry or wet conditions leads to a comparable catalytic behavior.

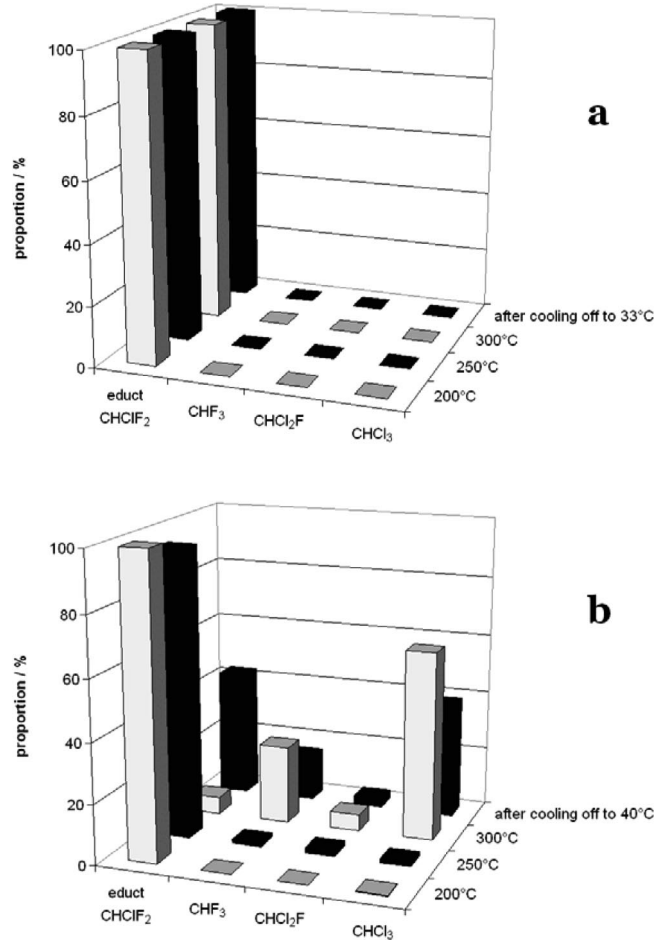

Figure 7. Product distribution obtained for the $CHClF_2$ dismutation reaction using milled and unmilled α-AlF_3 as catalysts: (a) unmilled α-AlF_3 and (b) 4 h milled α-AlF_3 (air). (Results obtained for the dry-milled sample are almost identical to those in b.)

The thermal behavior of unmilled and milled α-AlF_3 is quite different. The crystalline α-AlF_3 shows the typical

(40) Hess, A.; Kemnitz, E. *J. Catal.* **1994**, *149*, 449.
(41) EU project NMP3-CT-2004-5005575 (Funfluos).
(42) Krahl, T.; Stösser, R.; Kemnitz, E.; Scholz, G.; Feist, M.; Silly, G.; Buzaré, J. Y. *Inorg. Chem.* **2003**, *42*, 6474.

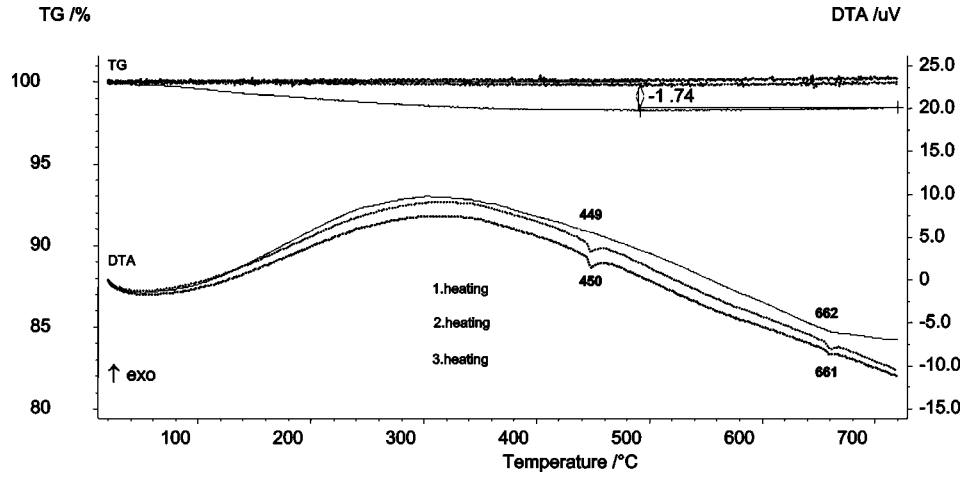

Figure 8. DTA-TG curves of the air-milled α-AlF_3 sample recorded with three consecutive heating and cooling cycles.

endothermal effect at 450 °C caused by the phase transition to the high-temperature cubic phase.[22–25] DTA-TG measurements with the milled samples permit the observation of this phase transition only during the second or every further heating cycle (cf. Figure 8).

Discussion

The results of the present study do not show the existence of an amorphous content in the milled samples. Even after prolongated milling times such as, for example, 16 h, the sample is nanocrystalline. This is different from results obtained after milling of many oxide materials such as, for example, corundum. In this case as one example for hard and non-flexible materials, the formation of an amorphous part can readily be observed at short milling periods.[9]

The main effect at milling is the formation of very small particles. Here, the two applied methods for particle size determination give consistent results. Whereas XRD gives the information of a mean particle size (45 nm in milled samples), TEM allows one to observe both smaller and larger particles around this average value.

The treatment of the milled sample in the thermobalance did not result in an accentuated exothermic effect responsible for crystallization effects, which should have been expected in going from amorphous to crystalline phases. Heating results in a grain growth, an agglomeration and healing up of defects of the nanoparticles indicated by a broad endothermal peak at 662 °C in the first heating run. The so-formed crystalline sample allows thereafter, beginning with the second heating cycle, the phase transition from the rhombohedral to the cubic phase, which is directly linked to the long-range order in the matrix (see Figure 8), to be observed.

The maximum ν_Q value of about 90 kHz for aluminum estimated for the milled samples by simulation is about three times larger than the value of unmilled α-AlF_3. Compared to the distribution of quadrupolar parameters of ^{27}A1 in aluminum chlorofluoride (ACF) ($\sigma = 440 \pm 40$ kHz) and amorphous AlF_3 ($\sigma = 360 \pm 40$ kHz),[42] this value is very small. Obviously, the absence of an amorphous part has the consequence of a smaller distribution width of the quadrupolar parameters. The latter can be in the present study only interpreted as a consequence of nanocrystallinity. The distribution of quadrupolar parameters is due to a distribution of electric field gradients in the milled samples. This fact can be related to surface distortions and unsaturated bonds in the surface of nanoparticles, which are finally responsible for the observed acidity and hardly detected with bulk methods. These results correlate nicely with indicated distributions of Al−F distances in plasma synthesized AlF_3 nanoparticles derived from pair distribution function analysis of XRD data.[27] The ^{19}F spin lattice relaxation time indicates sensitively the increased surface to bulk ratio in the milled samples. Obviously, the lowering of the spin lattice relaxation time at milling is a direct consequence of the rising number of lattice defects like unsaturated bonds introduced by milling, as well as an increased flexibility in the surface. Both may open additional relaxation channels for magnetization. These findings are similar to those obtained for mechanically activated CaF_2 samples.[18]

Milling of crystalline α-AlF_3 introduced a large number of distortions and with it active sites on the surface. TPD desorption and CO adsorption experiments proved the existence of Brønsted and Lewis acid sites. Their existence is not necessarily associated with a high surface area, which is not substantially increased by milling. A pre-treatment of the milled samples under mild conditions (90 °C, vacuum) does not remove all surface OH groups or water molecules. As a result the TPD profile of ammonia has a large area due to the combined action of Brønsted and Lewis acid sites. Although less strong, the number Lewis acid sites is doubled following the dry-milling route as indicated by CO adsorption measurements. The larger number on the one hand but weaker character of the Lewis acid sites on the other hand in the dry milled sample have evidently a compensating effect. As a consequence, the catalytic test reaction as indicator for the presence of Lewis acid sites proceeds successfully but with about the same conversion (see eq 1), Figure 7) as for the air-milled sample.

Present thermoanalytical investigations confirm results of MD simulations that no phase transition from the rhombohedral to the cubic phase is observed in the case of very small particles. Obviously, cooperative motions involving

rotations of the AlF_6 units[25] responsible for the phase transition require mean particle sizes much larger than about 40 nm.

Conclusions

The mechanical activation of α-AlF_3 results in considerable changes of particle sizes and shapes. Results of XRD as well as TEM indicate that the mechanically activated samples, under the conditions applied here, are nanocrystalline. Obviously, the cleavage of the crystallites is the dominating process at milling. These findings are supported by MAS NMR as bulk method giving no indication for an alteration of the sixfold fluorine coordination of aluminum in the bulk. The main modification observed with ^{27}A1 MAS NMR is the spread of the spinning side bands. This can only be interpreted in terms of a distribution of bond angles and lengths appearing in the nanosized milled samples. Such distributions may be induced by surface distortions and unsaturated bonds in the surface of the nanoparticles which are finally responsible for the catalytic activity of the milled samples. The maximum ν_Q value of aluminum is about three times larger than in the starting crystalline material, underlining the nanocrystalline state of the milled samples. The flexibility of the fluorine matrix prevents larger distortions. As already found out for milled CaF_2 samples[18] the ^{19}F spin lattice relaxation times give a sensitive indication for new relaxation channels in the mechanically activated samples opened by defects and a high flexibility in the surface of nanoparticles.

It could be unambiguously shown that milling generates acid sites. Dry-milling produces mainly Lewis acid sites whereas air-milling results in both Brønsted and Lewis acid sites.

Consequently, it could be evidenced for the first time that unlike crystalline α-AlF_3, milled, nanosized α-AlF_3 samples are catalytically active. The observed properties of nanocrystalline α-AlF_3 produced by milling experimentally confirm to the theoretically predicted Lewis acidity of cubic AlF_3 nanoparticles.[27]

Acknowledgment. S. Bässler is kindly acknowleged for DTA-TG measurements, S. Wuttke for CO adsorption experiments, Dr. M. Daturi (Caen) for giving access to the FT-IR cell and spectrometer, and A. Pawlik for the ^{27}A1 measurements at the 750 MHz spectrometer.

CM801135H